HHS Public Access

Author manuscript

J Neurol. Author manuscript; available in PMC 2017 March 28.

Published in final edited form as:

J Neurol. 2016 June ; 263(6): 1146–1155. doi:10.1007/s00415-016-8118-z.

Quantification of normal-appearing white matter tract integrity in multiple sclerosis: a diffusion kurtosis imaging study

Ivan de Kouchkovsky, BA[1], **Els Fieremans, PhD**[2], **Lazar Fleysher, PhD**[3], **Joseph Herbert, MD**[4], **Robert I. Grossman, MD**[2], and **Matilde Inglese, MD, PhD**[3,5]

[1]Medical Degree Program, New York University School of Medicine, New York, NY, USA

[2]Department of Radiology, Neurology (J.H.), New York University School of Medicine, New York, NY, USA

[3]Department of Radiology, Icahn School of Medicine at Mount Sinai, New York, NY, USA

[4]Department of Neurology, New York University School of Medicine, New York, NY, USA

[5]Department of Neurology and Neuroscience, Icahn School of Medicine at Mount Sinai, New York, NY, USA

Abstract

Our aim is to characterize the nature and extent of pathological changes in the normal-appearing white matter (NAWM) of patients with multiple sclerosis (MS) using novel diffusion kurtosis imaging-derived white matter tract integrity (WMTI) metrics, and to investigate the association between these WMTI metrics and clinical parameters. 32 patients with relapsing-remitting MS and 19 age- and gender-matched healthy controls underwent MRI and neurological examination. Maps of mean diffusivity, fractional anisotropy and WMTI metrics (intra-axonal diffusivity, axonal water fraction, tortuosity and axial and radial extra-axonal diffusivity) were created. Tract-based spatial statistics analysis was performed to assess for differences in the NAWM between patients and controls. A region of interest analysis of the corpus callosum was also performed to assess for group differences and to evaluate correlations between WMTI metrics and measures of disease severity. Mean diffusivity and radial extra-axonal diffusivity were significantly increased while fractional anisotropy, axonal water fraction, intra-axonal diffusivity and tortuosity were decreased in MS patients compared with controls (p values ranging from <0.001 to < 0.05). Axonal water fraction in the corpus callosum was significantly associated with the expanded disability status scale score ($\rho = -0.39$, $p = 0.035$). With the exception of the axial extra-axonal diffusivity, all metrics were correlated with the symbol digits modality test score (p values ranging from 0.001 to

Corresponding author: Matilde Inglese Department of Neurology, Radiology and Neuroscience, Icahn School of Medicine at Mount Sinai School of Medicine, New York, NY., matilde.inglese@mssm.edu, Telephone: 212-824-9310; Fax: 212-348-1310.

Ethical standards

This study was approved by the Institutional Board of Research Associates at the NYU School of Medicine, and was performed in accordance with the ethical standards laid down in the 1964 Declaration of Helsinki and its later amendments. Written informed consent was obtained from all subjects prior to their inclusion in this study.

Conflict of interest disclosures

Ivan de Kouchkovsky has nothing to disclose. Dr. Lazar Fleysher has nothing to disclose.
Dr. Els Fieremans has received research grants from NIH, ADDF and Avid Radiopharmaceuticals
Dr. Robert I. Grossman has nothing to disclose
Dr. Matilde Inglese has received research grants from NIH, NMSS, Novartis Pharmaceuticals Corp., Teva Neuroscience.

< 0.05). WMTI metrics are thus sensitive to changes in the NAWM of MS patients and might provide a more pathologically specific, clinically meaningful and practical complement to standard diffusion tensor imaging-derived metrics.

Keywords

multiple sclerosis; MRI; DTI; DKI; EDSS

Introduction

Multiple Sclerosis (MS) is the most common cause of non-traumatic disability in young adults and is characterized by white matter (WM) degeneration involving a spectrum of pathological processes, such as inflammation, demyelination, axonal loss, edema and remyelination [1–4]. This pathological heterogeneity is associated with substantial interpatient variability in disease burden and progression, and likely contributes to the absence of rigorous clinical markers of prognosis [5]. Although conventional MRI plays an important role in the diagnosis of MS, it has a low pathological specificity and correlates poorly with disease burden [6]. The successful management of MS and monitoring of treatment response thus call for new markers with an increased sensitivity and specificity for the disease's various pathological processes. Unlike conventional MRI, diffusion MRI techniques, including diffusion tensor imaging (DTI) and diffusional kurtosis imaging (DKI) [7], are sensitive to diffuse microscopic injury in the normal-appearing white matter (NAWM) and gray matter of MS patients [8–10]. Both DTI and DKI metrics, however, are empirical diffusion measures and lack microstructural and pathological specificity [7]. We have previously introduced a diffusion model of WM [11] (Fig. 1) that is suitable for DKI analysis and allows for the quantification of the intra- (D_{axon}) and extra-axonal diffusivities (both radial and axial $D_{e,radial}$ and $D_{e,axial}$, respectively), the axonal water fraction (AWF) and the tortuosity of the extra-axonal space. These WM tract integrity (WMTI) metrics may be more specific than standard DTI- and DKI-parameters to the different pathological processes involved in MS. The aims of this study were to determine the presence and extent of changes in WMTI metrics in the NAWM of patients with relapsing-remitting MS (RRMS) and to investigate the association between WMTI metrics, disease duration and clinical disability.

Methods

Subjects

Thirty-two patients with clinically definite MS [12] (8 males and 24 females) were prospectively enrolled from the MS center of the New York University (NYU) medical center (Table 1). Inclusion criteria consisted of a relapsing-remitting course [13] and a relapse- and steroid treatment-free period of at least three months prior to study entry. Patients with other relevant diseases or contraindications to performing MRI were excluded. Neurological assessment included the expanded disability status scale (EDSS) [14] and symbol digit modality test (SDMT) [15]. Patients had a mean age of 37.0 ± 9.3 years; a mean disease duration (from the date of diagnosis to MRI acquisition) of 3.6 ± 3.9 years and

a median EDSS score of 2.0 (range 0–6). All but three patients were on a disease modifying agent at the time of this study: Eleven on interferon beta-1a, five on interferon beta-1b, six on glatiramer aceatate, six on natalizumab, and one on rituximab. For comparison, nineteen age and sex-matched healthy controls (HC; 6 males and 13 females; mean age 36.2 ± 11.4) with no known brain abnormalities and no neurological symptoms were recruited. Approval for this study was received from the local Institutional Board of Research Associates and written informed consent was obtained from all subjects.

MRI acquisition

All subjects underwent MRI on a Siemens Tim Trio MRI scanner (Siemens, Erlangen. Germany) with a 12-channel head coil. MS patients received a standard-dose (0.1 mmol/kg) bolus of gadopentetatedimeglumine (Gd; Magnevist; Berlex Laboratories, Wayne, NJ) injection after acquisition of the DKI sequences. The MRI protocol included (1) axial T2-weighted dual-echo turbo spin-echo (TSE) sequence (repetition time (TR): 6570 ms, echo time (TE): 101 ms, 50 contiguous 3-mm thick slices); (2) a sagittal T1-weighted 3D MPRAGE sequence pre - and post-Gd injection (TR/TE: 1360/2.6 ms, inversion time (TI): 800 ms, spatial resolution: $1\times1\times1$ mm^3); (3) an axial T2 fluid-attenuated inversion recovery (FLAIR) sequence (TR/TE/TI: 9000/87/2500 ms, 50 3-mm thick slices); (4) a twice-refocused spin echo EPI sequence for DKI with b-values of 1000 and 2000 s/mm^2 and 30 directions each (repeated twice), in addition to 11 $b = 0$ images (TR/TE: 3700/96 ms, FOV of 222×222 mm^2, matrix 82×82, 28 axial 2.7-mm thick slices).

Lesion count and volume assessment

Quantification of Gd contrast enhancing lesion number (CE), T2-hyperintense and T1-hypointense lesion volume (T2LV and T1LV, respectively) was performed in each patient by a single experienced observer unaware of subject identity, employing a segmentation technique based on user-supervised local thresholding (Jim 3.0, Xinapse System, Leicester, UK) [16].

Image processing and white matter tract integrity metrics

Diffusion MRI data was transferred to an offline workstation and processed using in-house developed software in Matlab (R2015a, Math Works, Inc, Natick, MA) to derive parametric maps of the conventional DTI metrics of mean diffusivity (MD), and fractional anisotropy (FA) [17]. We have previously introduced a WM diffusion model that allows for a direct interpretation of DKI metrics in terms of WM microstructure. The model assumes that axons are relatively parallel impermeable sticks (cylinders with effective zero radius), thereby dividing the WM microstructure into myelin and two non-exchanging water compartments —the intra- and extra-axonal spaces (Fig. 1). Based on previously published mathematical derivations [11], the following WM tract integrity metrics were derived from DKI for a coherently aligned single fiber bundle:

- The axonal water fraction (AWF), which represent the ratio of water within the intra-axonal space over the total amount of water (i.e. water in the intra- and extra-axonal space). It should be noted that water inside the myelin is not

detected with a typical diffusion acquisition, and hence not included in the model. This metric is thought to be a potential marker of axonal loss [18];

- The intra-axonal diffusivity (D_{axon}), which corresponds to the diffusivity of water inside of axons, and is assumed to be entirely restricted to the direction of axonal tracts (i.e. in the axial direction only). It is a potential marker of intra-axonal injury [19];
- The axial and radial extra-axonal diffusivities ($D_{e,axial}$ and $D_{e,radial}$, respectively), which quantify diffusivity in the extracellular space parallel (i.e. axial) to and perpendicular (i.e. radial) to axonal tracts. Unlike D_{axon}, these metrics are specific for extra-axonal processes and represent potential markers of extracellular inflammation, gliosis, and demyelination;
- Lastly, the tortuosity of the extra-axonal space, which is defined as the ratio of intrinsic diffusivity in the extra-axonal space (which we approximate as the axial extra-axonal diffusivity) over diffusivity in the extra-axonal space perpendicular to axonal tracts (i.e. $D_{e,axial}$ over $D_{e,radial}$,). It is a potential marker of demyelination [18].

Tract-Based Spatial Statistics Analysis

Voxelwise statistical analysis of the FA data was carried out using TBSS (Tract-Based Spatial Statistics[20], part of FSL (FMRIB Software Library)[21]. All subjects' FA maps were registered to FMRIB58 FA template with the nonlinear registration tool FNIRT[22] and resampled to $1\times1\times1mm^3$ Montreal Neurological Institute152 space. All other parametric maps underwent the same transformations for subsequent processing. Next, a mean FA image was created and thinned to create a mean FA skeleton representing the centers of all tracts common to the group. The FA skeleton was thresholded to $FA \geq 0.4$ to restrict further analysis to WM regions consisting of single-fiber bundles. All parametric maps of each subject were then projected onto this FA skeleton for further skeletonized voxelwise statistical analysis. TBSS analysis was performed across all voxels on the skeleton by using a permutation-based interference tool for nonparametric statistical thresholding (Randomise;FSL). Between-group comparisons of all parameters within the skeleton were tested by using *t* tests, with subject age and gender as a covariate. The number of permutations was set to 10,000. The resulting statistical maps were thresholded (two-sided $P < 0.05$), with correction for multiple comparisons included by using the threshold-free cluster enhancement option [23]. Additionally, lesion masks were created for each patient on axial FLAIR images, transformed in standard space and averaged to create a mean lesion mask across all patients. This was then thresholded to include only voxels in which at least 10% of patients had a lesion.

Regions of Interest Analysis

Regions of Interest (ROI) analysis was performed to investigate group differences and correlations between DKI-derived metrics and measures of disease burden and severity. ROI analysis was restricted to the corpus callosum (CC), whose well-ordered axonal tracts best correspond to the WM model used to derive our WMTI metrics. ROIs for the genu, body

and splenium of the CC were selected from the ICBM-DTI-81 white-matter labels atlas. For every subject, mean values and standard deviations of MD, FA, AWF, D_{axon}, $D_{e,axial}$, $D_{e,radial}$, and tortuosity were calculated in each ROI (voxels corresponding to a T2-hyperintense lesion were excluded from patients' ROIs). Analysis of covariance was performed (using Matlab's "aoctool" function) to identify statistically significant group differences between HC and RRMS after correcting for age (two-sided $P < 0.05$). Pearson linear correlation coefficients between mean ROIs metric values and SDMT, DD, T2LV, T1LV and CE were derived using Matlab's "partialcorr" function. Correlations with SDMT, T2LV, T1LV and CE were corrected for age, gender and disease duration. One patient with significantly higher T2LV and T1LV was identified as an outlier and removed from the correlation analyses. Correlations with EDSS, which is an ordinal measure, were evaluated in each ROI using Spearman rank correlation after correcting for age, gender and disease duration. Given the exploratory nature of this study, statistical significance was defined as $P < 0.05$, and adjustments for multiple comparisons were not performed. Lastly, a receiver operating characteristics (ROC) curve analysis was performed to assess the performance of each DTI and WMTI metrics in discriminating between RRMS patients and HC. Mean values of all seven metrics were obtained for each ROI, excluding any voxels corresponding to a T2-hyperintense lesion. For each metrics, Matalab's "perfcurve" function was used to plot an ROC curve and to calculate the area under the curve (AUC) as well as the sensitivity and specificity of the optimal operating point of the ROC curve.

Results

TBSS Analysis

TBSS analysis revealed widespread differences in the NAWM skeleton of RRMS patients compared to that of HC (Fig. 2). With the exception of $D_{e,axial}$, changes in WMTI metrics were observed throughout the NAWM, including the CC, internal capsules, cerebral peduncles and posterior thalamic radiations (Fig. 2, c–f). Values of MD, as well as the WMTI metric of $D_{e,radial}$ were increased in RRMS patients compared to HC, with statistically significant differences in 82.4 and 43.3% of NAWM-skeleton voxels, respectively. On the other hand FA and the WMTI metrics of D_{axon}, AWF and tortuosity were decreased in RRMS patients, with statistically significant differences in 66.8, 4.0, 79.4 and 46.1% of NAWM-skeleton voxels, respectively. 78% of NAWM-skeleton voxels had a concomitant change in MD one of the five WMTI metrics, while only 65% had a change in both FA and one of the WMTI metrics. We observed a significant overlap between changes in MD and AWF (changes in both metrics were observed in 74% of all voxels), with diffuse involvement of the NAWM and relative sparing of the anterior limbs of the internal capsule. Changes in AWF and $D_{e,radial}$ were more likely to be associated with a concomitant change in MD, while changes in tortuosity and D_{axon} tended to overlap more with a change in FA. Compared to MD, AWF and FA, significant changes in $D_{e,radial}$ and tortuosity were mostly confined to the posterior NAWM tracts, which also corresponded to the areas with the highest lesion load in our patient cohort. The observed decrease in D_{axon} was limited to the body and splenium of the CC, the left retrolenticular part of the internal capsule and the left posterior thalamic radiation (Fig. 2, b). All of the voxels with a significant decrease in D_{axon}

corresponded to voxels with a concomitant decrease in AWF and FA. No significant differences were found in the axial extra-axonal diffusivity (Fig. 3).

ROI Analysis: Group Differences and ROC Curves

Mean values and standard deviations for MD, FA and the five WMTI metrics in the genu, body and splenium of the CC of HC and RRMS subjects are summarized in table 2. P-values from the analysis of covariance (correcting for age) are also included. The standard deviation for both conventional DTI and WMTI metrics ranges from 3% to 15% of the mean ROI value. In accordance with the results of our TBSS analysis, analysis of the CC yielded statistically significant group differences in MD, FA, AWF, $D_{e,radial}$ and tortuosity: Mean values of MD and $D_{e,radial}$ were increased in RRMS patients (with p-values ranging from 0.002–0.016 and 0.008–0.030, respectively), while FA, AWF and tortuosity were decreased when compared to HC (p-values ranging from 0.014–0.048, <0.001–0.004, and 0.002–0.012, respectively). No statistically significant difference was observed in mean D_{axon} and $D_{e,axial}$ across the two groups. The area under the ROC curve (AUC) for each metric in the genu, body and splenium of the CC is reported in table 2. Of the conventional DTI metrics, MD showed the highest performance, with an AUC of 0.79 in the splenium of the CC and a sensitivity and specificity (at the optimal operating point of the ROC curve) of 91% and 58%, respectively. Of the five WMTI metrics, AWF in the body of the CC was best at differentiating RRMS patients from HC with an AUC of 0.85, a lower sensitivity of 79% and a higher specificity of 78% at the optimal point of the ROC curve.

ROI Analysis: Correlations with disease burden and severity

A statistically significant Spearman rank correlation between AWF and EDSS was found in the body of the CC, with a coefficient of −0.39 ($p = 0.035$; Fig. 4). Additionally, correlations between EDSS and MD and FA in the body approached statistical significance ($\rho = 0.36$, $p = 0.055$ and $\rho = -0.36$, $p = 0.052$, respectively). With the exception of $D_{e,axial}$, all metrics correlated with cognitive impairment as measured by SDMT score. MD and $D_{e,radial}$ in the CC were negatively correlated with SDMT, with coefficients ranging from −0.45 ($p = 0.015$) to −0.51 ($p = 0.005$) and −0.44 ($p = 0.017$) to −0.51 ($p = 0.005$), respectively. FA, AWF, D_{axon} and tortuosity were all positively correlated with SDMT. DD was negatively correlated to FA, AWF and tortuosity across all regions of the CC ($p < 0.001$, < 0.001 and < 0.03, respectively), while MD, $D_{e,axial}$ and $D_{e,radial}$ increased with increasing DD ($p < 0.003$). No correlation was found between DD and D_{axon}. T2LV and T1LV were positively correlated with MD and $D_{e,radial}$ in the splenium, and negatively correlated with FA, AWF and D_{axon} in the splenium. Additionally, both were negatively correlated with AWF in the body. With the exception of D_{axon} in the genu ($\rho = -0.38$, $p = 0.041$), no significant correlations were found between any of the metrics and CE (Online Resource 1).

Discussion

In this study, we sought to demonstrate the utility of recently proposed DKI-derived WM tract integrity metrics [24] in characterizing the various pathological changes occurring in the NAWM of patients with RRMS. We thereby hypothesized an increased pathological specificity of WMTI metrics in MS, including an increased specificity to the clinically

significant processes that underlie disease burden and disability. While histological confirmation in MS pathology is lacking, several recent animal validation and pilot patient studies have suggested that WMTI metrics potentially can disentangle intra-, and extra-axonal processes and higher specificity to underlying disease mechanisms. Indeed, recent studies of cuprizone-induced demyelination in mice have shown very good correlations between WMTI metrics and histological measurements [25–27]. Most notably, mean AWF in the corpus callosum of mice fed a cuprizone diet is strongly correlated with tissue axonal water fraction (as measured by electron microscopy) but not with the g-ratio (the ratio of the inner axonal diameter to the total outer diameter, a marker of demyelination). On the other hand, mean $D_{e,radial}$ increases with increasing g-ratio, but is not correlated to tissue axonal water fraction [27]. Furthermore, an *in vivo* study of patients with mild traumatic brain injury has also shown that levels of N-acetyl-aspartate—a "gold standard" metric for neuroaxonal damage—are associated with the WMTI metrics of intra- and extra-axonal damage (AWF, D_{axon}, $D_{e,radial}$ and tortuosity) [28]. In normal early human development, we have previously demonstrated a non-linear increase in AWF and tortuosity that is consistent with expected behavior related to myelination and asynchrony of fiber development [29]. WMTI metrics have also been applied to the study of other neurodegenerative disorders such as stroke [19] and Alzheimer's disease, where they have shown sensitivity to different stages in the disease course [30] and have been used to highlight the vulnerability of late-myelinating versus early-myelinating tracts in Alzheimer's Disease [31].

Here, we report widespread decreased FA and increased MD in the NAWM of MS patients, which confirm previous studies [32,33] and extend these by demonstrating the presence, extent and clinical impact of abnormal values of the intra-axonal diffusivity (D_{axon}), axial and radial extra-axonal diffusivities ($D_{e,axial}$ and $D_{e,radial}$), axonal water fraction (AWF), and tortuosity of the extra-axonal space.

There is extensive histopathological and MRI evidence that NAWM is affected, albeit to a lesser extent, by the same pathological processes that characterize WM lesions—inflammation, demyelination, axonal injury, macrophages infiltration and gliosis [34,2–4]. Quantitative in vivo MR techniques, including measures of magnetization transfer, diffusion, relaxation times and spectroscopic metabolite concentrations, have revealed that NAWM abnormalities are present from clinical onset and become more pronounced with clinical progression and increase of lesion load and disability [35]. The widespread NAWM increase of radial extra-axonal diffusivity and decrease of tortuosity and AWF observed both in the TBSS and the ROI analysis of the patients' CC may reflect these various processes, such as demyelination (increased $D_{e,radial}$ and decreased tortuosity) and chronic axonal degeneration and loss (decreased AWF). Finally, the presence of significant correlations between the SDMT score—a measure of processing speed, attention and working memory—and WMTI metrics specific for demyelination and axonal damage supports the concept that, at least in part, the clinical-radiological paradox is due to the lack of pathological specificity of conventional MRI measures.

It has been demonstrated that NAWM abnormalities develop, to an extent, as a consequence of Wallerian degeneration of axons transected by focal demyelination within near or distant WM lesions [36]. This is supported by the significant association between WMTI metrics

(particularly AWF) and T2- and T1-lesion loads found in our study. However, in line with previous findings in the literature, the association with lesion load is far from perfect and suggests that NAWM abnormalities are partly independent of lesions. Indeed, NAWM pathology may develop for many weeks, months and even years prior to focal lesion development suggesting the presence of pre-existing processes such as microglial activation and/or low-grade blood brain barrier inflammation that can predispose to lesion formation [37]. Due to the cross-sectional nature of our study, we cannot support the presence of pre-lesional damage; however, the use of WMTI metrics in longitudinal studies will help clarify the pathological background of pre-lesional WM tissue changes.

The intra-axonal diffusivity D_{axon} has been advanced as a potential marker of acute intra-axonal injury, and has been observed to decrease following stroke [19] and mild traumatic brain injury [28]. In a recent temporal study of WMTI metrics, D_{axon} was found to be significantly decreased in the body and splenium of the CC of mice after a 3-week period of cuprizone diet (during the acute inflammatory response to cuprizone), while no change was observed after a 6-week period of cuprizone diet or a 6-week period of cuprizone diet followed by 6 weeks of recovery [26]. AWF on the other hand did not decrease until 6 weeks of cuprizone exposure, and remained low throughout the recovery period. In our present study, unlike AWF, $D_{e,radial}$ and tortuosity, D_{axon} did not show any association with disease duration. Interestingly, D_{axon} was decreased in a small percentage of NAWM voxels in our TBSS analysis as well as in our ROI analysis of the CC (although the later failed to reach statistical significance when compared to HC). This decrease in D_{axon} may reflect ongoing subclinical disease activity in a subset of patients, as evidenced by the presence of contrast enhancing lesions in 12 out of the 32 enrolled patients, as well as the modest negative correlation observed between D_{axon} and CE ($\rho = -0.38$, $p = 0.041$).

Although MD, FA and AWF all showed widespread differences in the NAWM skeleton of patients with RRMS, AWF was the only metric associated with clinical disability as measured by EDSS score. Thus while all three metrics were altered in the NAWM, AWF may be more specific and therefore more sensitive to the underlying pathological processes responsible for clinical disability in RRMS. Indeed, AWF has been suggested to be uniquely sensitive to chronic axonal degeneration and loss [18,38]. Hence, our finding supports the role for WMTI metrics as a more specific set of markers of WM pathology. This study is not without limitations. The image acquisition protocol used in this study only provided partial coverage of the brain, excluding portions of the cerebral peduncles. It is an exploratory study with a relatively small number of subjects, and is inherently limited by the cross-sectional nature of its design. Although a growing body of literature suggests an increased specificity of WMTI metrics to various pathological processes, many such processes are likely taking place at once in the NAWM of patients with MS. Longitudinal data would be needed to explore the relationship between the changes observed in various metrics, such as D_{axon}, tortuosity and AWF, and disease progression. Similarly, histopathological correlation would ultimately be needed to fully interpret changes in WMTI metrics. Lastly, it is important to note that the WM model used to derive our WMTI metrics relies on several, albeit common assumptions regarding the WM microstructure. In particular, it assumes that $D_{axon} < D_{e,axial}$, and that axonal fibers are organized in a relatively parallel fashion along a single direction. In order to maximally respect this latter assumption, the NAWM skeleton used for our TBSS

analysis was thresholded to exclude voxels with low FA, and our ROI analysis was limited to the CC after excluding all T2-intense lesions. Still, these measures do not guarantee that all axonal fibers are perfectly aligned within a single voxel. The tortuosity of the extra-axonal space, which we derive by equating the intrinsic extra-axonal diffusivity to $D_{e,axial}$, is most susceptible to this assumption.

Nevertheless, there remains a huge need for pathologically specific metrics able to predict the course of the disease and the response to available and experimental therapies. Here, we present the first reported study of WMTI metrics in the NAWM of patients with MS. Our findings suggest that these novel metrics might provide a more pathologically specific complement to standard diffusion tensor imaging derived metrics. By better differentiating between acute axonal injury, chronic axonal degeneration and demyelination, these metrics may allow for a better characterization and understanding of disease progression and pathological variation among different MS subtypes. Further longitudinal study is also warranted to explore the role of WMTI metrics in predicting individual disease course and symptom progression.

Supplementary Material

Refer to Web version on PubMed Central for supplementary material.

Acknowledgments

This study was supported in part by National Multiple Sclerosis Society (NMSS RG 5120A3/1), the Noto Foundation to Inglese M, and by the National Institute of Neurological Disorders and Stroke of the National Institutes of Health under award number R01NS088040 to Fieremans E.

References

1. Lassmann H, Bruck W, Lucchinetti C. Heterogeneity of multiple sclerosis pathogenesis: implications for diagnosis and therapy. Trends Mol Med. 2001; 7(3):115–121. [PubMed: 11286782]
2. Trapp BD, Peterson J, Ransohoff RM, Rudick R, Mork S, Bo L. Axonal transection in the lesions of multiple sclerosis. N Engl J Med. 1998; 338(5):278–285. DOI: 10.1056/NEJM199801293380502 [PubMed: 9445407]
3. Evangelou N, Esiri MM, Smith S, Palace J, Matthews PM. Quantitative pathological evidence for axonal loss in normal appearing white matter in multiple sclerosis. Ann Neurol. 2000; 47(3):391–395. [PubMed: 10716264]
4. Evangelou N, Konz D, Esiri MM, Smith S, Palace J, Matthews PM. Regional axonal loss in the corpus callosum correlates with cerebral white matter lesion volume and distribution in multiple sclerosis. Brain. 2000; 123(Pt 9):1845–1849. [PubMed: 10960048]
5. Confavreux C, Vukusic S, Adeleine P. Early clinical predictors and progression of irreversible disability in multiple sclerosis: an amnesic process. Brain. 2003; 126(Pt 4):770–782. [PubMed: 12615637]
6. Klawiter EC. Current and new directions in MRI in multiple sclerosis. Continuum (Minneap Minn). 2013; 19(4 Multiple Sclerosis):1058–1073. DOI: 10.1212/01.CON.0000433283.00221.37 [PubMed: 23917101]
7. Jensen JH, Helpern JA. MRI quantification of non-Gaussian water diffusion by kurtosis analysis. NMR Biomed. 2010; 23(7):698–710. DOI: 10.1002/nbm.1518 [PubMed: 20632416]
8. Inglese M, Bester M. Diffusion imaging in multiple sclerosis: research and clinical implications. NMR Biomed. 2010; 23(7):865–872. DOI: 10.1002/nbm.1515 [PubMed: 20882528]

9. Yoshida M, Hori M, Yokoyama K, Fukunaga I, Suzuki M, Kamagata K, Shimoji K, Nakanishi A, Hattori N, Masutani Y, Aoki S. Diffusional kurtosis imaging of normal-appearing white matter in multiple sclerosis: preliminary clinical experience. Jpn J Radiol. 2013; 31(1):50–55. DOI: 10.1007/s11604-012-0147-7 [PubMed: 23086313]
10. Bester M, Jensen JH, Babb JS, Tabesh A, Miles L, Herbert J, Grossman RI, Inglese M. Non-Gaussian diffusion MRI of gray matter is associated with cognitive impairment in multiple sclerosis. Mult Scler. 2015; 21(7):935–944. DOI: 10.1177/1352458514556295 [PubMed: 25392318]
11. Fieremans E, Jensen JH, Helpern JA. White matter characterization with diffusional kurtosis imaging. Neuroimage. 2011; 58(1):177–188. DOI: 10.1016/j.neuroimage.2011.06.006 [PubMed: 21699989]
12. Polman CH, Reingold SC, Banwell B, Clanet M, Cohen JA, Filippi M, Fujihara K, Havrdova E, Hutchinson M, Kappos L, Lublin FD, Montalban X, O'Connor P, Sandberg-Wollheim M, Thompson AJ, Waubant E, Weinshenker B, Wolinsky JS. Diagnostic criteria for multiple sclerosis: 2010 revisions to the McDonald criteria. Ann Neurol. 2011; 69(2):292–302. DOI: 10.1002/ana.22366 [PubMed: 21387374]
13. Lublin FD, Reingold SC. Defining the clinical course of multiple sclerosis: results of an international survey. National Multiple Sclerosis Society (USA) Advisory Committee on Clinical Trials of New Agents in Multiple Sclerosis. Neurology. 1996; 46(4):907–911. [PubMed: 8780061]
14. Kurtzke JF. A new scale for evaluating disability in multiple sclerosis. Neurology. 1955; 5(8):580–583. [PubMed: 13244774]
15. Benedict RH, Fischer JS, Archibald CJ, Arnett PA, Beatty WW, Bobholz J, Chelune GJ, Fisk JD, Langdon DW, Caruso L, Foley F, LaRocca NG, Vowels L, Weinstein A, DeLuca J, Rao SM, Munschauer F. Minimal neuropsychological assessment of MS patients: a consensus approach. Clin Neuropsychol. 2002; 16(3):381–397. DOI: 10.1076/clin.16.3.381.13859 [PubMed: 12607150]
16. Inglese M, Madelin G, Oesingmann N, Babb JS, Wu W, Stoeckel B, Herbert J, Johnson G. Brain tissue sodium concentration in multiple sclerosis: a sodium imaging study at 3 tesla. Brain. 2010; 133(Pt 3):847–857. DOI: 10.1093/brain/awp334 [PubMed: 20110245]
17. Tabesh A, Jensen JH, Ardekani BA, Helpern JA. Estimation of tensors and tensor-derived measures in diffusional kurtosis imaging. Magn Reson Med. 2011; 65(3):823–836. DOI: 10.1002/mrm.22655 [PubMed: 21337412]
18. Fieremans, E., Jensen, JH., Helpern, JA., Kim, S., Grossman, RI., Inglese, M., Novikov, DS. Diffusion distinguishes between axonal loss and demyelination in brain white matter. Proceedings of the 20th Annual Meeting of the International Society for Magnetic Resonance in Medicine; 2012.
19. Hui ES, Fieremans E, Jensen JH, Tabesh A, Feng W, Bonilha L, Spampinato MV, Adams R, Helpern JA. Stroke assessment with diffusional kurtosis imaging. Stroke. 2012; 43(11):2968–2973. DOI: 10.1161/STROKEAHA.112.657742 [PubMed: 22933581]
20. Smith SM, Jenkinson M, Johansen-Berg H, Rueckert D, Nichols TE, Mackay CE, Watkins KE, Ciccarelli O, Cader MZ, Matthews PM, Behrens TE. Tract-based spatial statistics: voxelwise analysis of multi-subject diffusion data. Neuroimage. 2006; 31(4):1487–1505. DOI: 10.1016/j.neuroimage.2006.02.024 [PubMed: 16624579]
21. Smith SM, Jenkinson M, Woolrich MW, Beckmann CF, Behrens TE, Johansen-Berg H, Bannister PR, De Luca M, Drobnjak I, Flitney DE, Niazy RK, Saunders J, Vickers J, Zhang Y, De Stefano N, Brady JM, Matthews PM. Advances in functional and structural MR image analysis and implementation as FSL. Neuroimage. 2004; 23(Suppl 1):S208–219. DOI: 10.1016/j.neuroimage.2004.07.051 [PubMed: 15501092]
22. Andersson, JLR., Jenkinson, M., Smith, S. Non-linear registration aka Spatial normalisation. FMRIB Centre; Oxford, UK: 2007.
23. Smith SM, Nichols TE. Threshold-free cluster enhancement: addressing problems of smoothing, threshold dependence and localisation in cluster inference. Neuroimage. 2009; 44(1):83–98. DOI: 10.1016/j.neuroimage.2008.03.061 [PubMed: 18501637]

24. Fieremans E, Jensen JH, Helpern JA. White matter characterization with diffusional kurtosis imaging. Neuroimage. 2011; 58(1):177–188. DOI: 10.1016/j.neuroimage.2011.06.006 [PubMed: 21699989]
25. Falangola MF, Guilfoyle DN, Tabesh A, Hui ES, Nie X, Jensen JH, Gerum SV, Hu C, LaFrancois J, Collins HR, Helpern JA. Histological correlation of diffusional kurtosis and white matter modeling metrics in cuprizone-induced corpus callosum demyelination. NMR Biomed. 2014; 27(8):948–957. DOI: 10.1002/nbm.3140 [PubMed: 24890981]
26. Guglielmetti C, Veraart J, Roelant E, Mai Z, Daans J, Van Audekerke J, Naeyaert M, Vanhoutte G, Delgado YPR, Praet J, Fieremans E, Ponsaerts P, Sijbers J, Van der Linden A, Verhoye M. Diffusion kurtosis imaging probes cortical alterations and white matter pathology following cuprizone induced demyelination and spontaneous remyelination. Neuroimage. 2016; 125:363–377. DOI: 10.1016/j.neuroimage.2015.10.052 [PubMed: 26525654]
27. Jelescu IO, Zurek M, Winters KV, Veraart J, Rajaratnam A, Kim NS, Babb JS, Shepherd TM, Novikov DS, Kim SG, Fieremans E. In vivo quantification of demyelination and recovery using compartment-specific diffusion MRI metrics validated by electron microscopy. Neuroimage. 2016; 132:104–114. DOI: 10.1016/j.neuroimage.2016.02.004 [PubMed: 26876473]
28. Grossman EJ, Kirov II, Gonen O, Novikov DS, Davitz MS, Lui YW, Grossman RI, Inglese M, Fieremans E. N-acetyl-aspartate levels correlate with intra-axonal compartment parameters from diffusion MRI. NeuroImage. 2015; 118(0):334–343. doi:http://dx.doi.org/10.1016/j.neuroimage.2015.05.061. [PubMed: 26037050]
29. Jelescu IO, Veraart J, Adisetiyo V, Milla SS, Novikov DS, Fieremans E. One diffusion acquisition and different white matter models: How does microstructure change in human early development based on WMTI and NODDI? Neuroimage. 2015; 107:242–256. DOI: 10.1016/j.neuroimage.2014.12.009 [PubMed: 25498427]
30. Fieremans E, Benitez A, Jensen JH, Falangola MF, Tabesh A, Deardorff RL, Spampinato MV, Babb JS, Novikov DS, Ferris SH, Helpern JA. Novel white matter tract integrity metrics sensitive to Alzheimer disease progression. AJNR Am J Neuroradiol. 2013; 34(11):2105–2112. DOI: 10.3174/ajnr.A3553 [PubMed: 23764722]
31. Benitez A, Fieremans E, Jensen JH, Falangola MF, Tabesh A, Ferris SH, Helpern JA. White matter tract integrity metrics reflect the vulnerability of late-myelinating tracts in Alzheimer's disease. NeuroImage: Clinical. 2014; 4(0):64–71. doi:http://dx.doi.org/10.1016/j.nicl.2013.11.001. [PubMed: 24319654]
32. Ceccarelli A, Rocca MA, Falini A, Tortorella P, Pagani E, Rodegher M, Comi G, Scotti G, Filippi M. Normal-appearing white and grey matter damage in MS. A volumetric and diffusion tensor MRI study at 3.0 Tesla. J Neurol. 2007; 254(4):513–518. DOI: 10.1007/s00415-006-0408-4 [PubMed: 17401516]
33. Mesaros S, Rocca MA, Riccitelli G, Pagani E, Rovaris M, Caputo D, Ghezzi A, Capra R, Bertolotto A, Comi G, Filippi M. Corpus callosum damage and cognitive dysfunction in benign MS. Hum Brain Mapp. 2009; 30(8):2656–2666. DOI: 10.1002/hbm.20692 [PubMed: 19067325]
34. Allen IV, McQuaid S, Mirakhur M, Nevin G. Pathological abnormalities in the normal-appearing white matter in multiple sclerosis. Neurol Sci. 2001; 22(2):141–144. [PubMed: 11603615]
35. Filippi M, Rocca MA, Barkhof F, Bruck W, Chen JT, Comi G, DeLuca G, De Stefano N, Erickson BJ, Evangelou N, Fazekas F, Geurts JJ, Lucchinetti C, Miller DH, Pelletier D, Popescu BF, Lassmann H. Attendees of the Correlation between Pathological MRIfiMSw. Association between pathological and MRI findings in multiple sclerosis. Lancet Neurol. 2012; 11(4):349–360. DOI: 10.1016/S1474-4422(12)70003-0 [PubMed: 22441196]
36. Droby A, Fleischer V, Carnini M, Zimmermann H, Siffrin V, Gawehn J, Erb M, Hildebrandt A, Baier B, Zipp F. The impact of isolated lesions on white-matter fiber tracts in multiple sclerosis patients. Neuroimage Clin. 2015; 8:110–116. DOI: 10.1016/j.nicl.2015.03.003 [PubMed: 26106534]
37. Varga AW, Johnson G, Babb JS, Herbert J, Grossman RI, Inglese M. White matter hemodynamic abnormalities precede sub-cortical gray matter changes in multiple sclerosis. J Neurol Sci. 2009; 282(1–2):28–33. DOI: 10.1016/j.jns.2008.12.036 [PubMed: 19181347]

38. Novikov, DS., Fieremans, E. Relating extracellular diffusivity to cell size distribution and packing density as applied to white matter. 20th Annual Meeting of the International Society for Magnetic Resonance in Medicine; 2012.

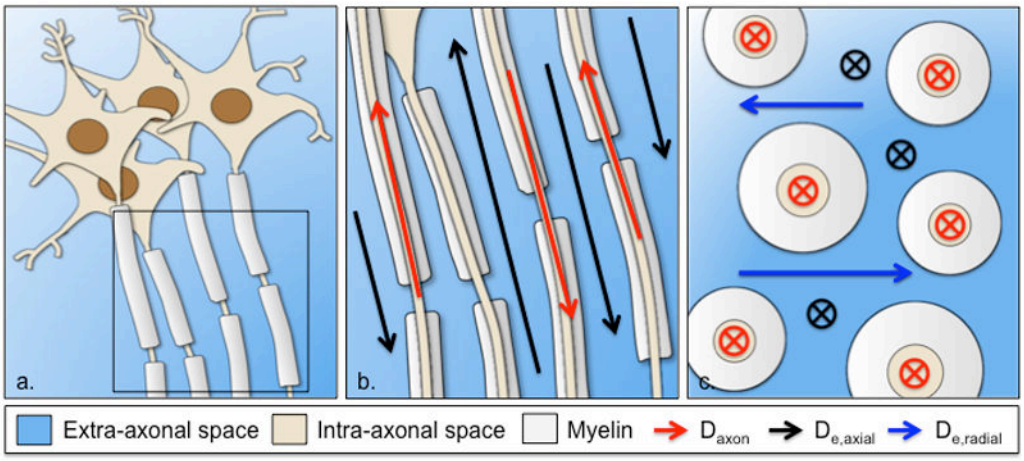

Fig. 1.

Schematic representation of the white matter as extra-axonal space and impermeable axons surrounded by myelin (a). Parallel view of an axonal fiber bundle with intra-axonal diffusivity and axial extra-axonal diffusivity along axonal tracts (b). Transverse view of an axonal fiber bundle showing the radial extra-axonal diffusivity perpendicular to axonal tracts (c)

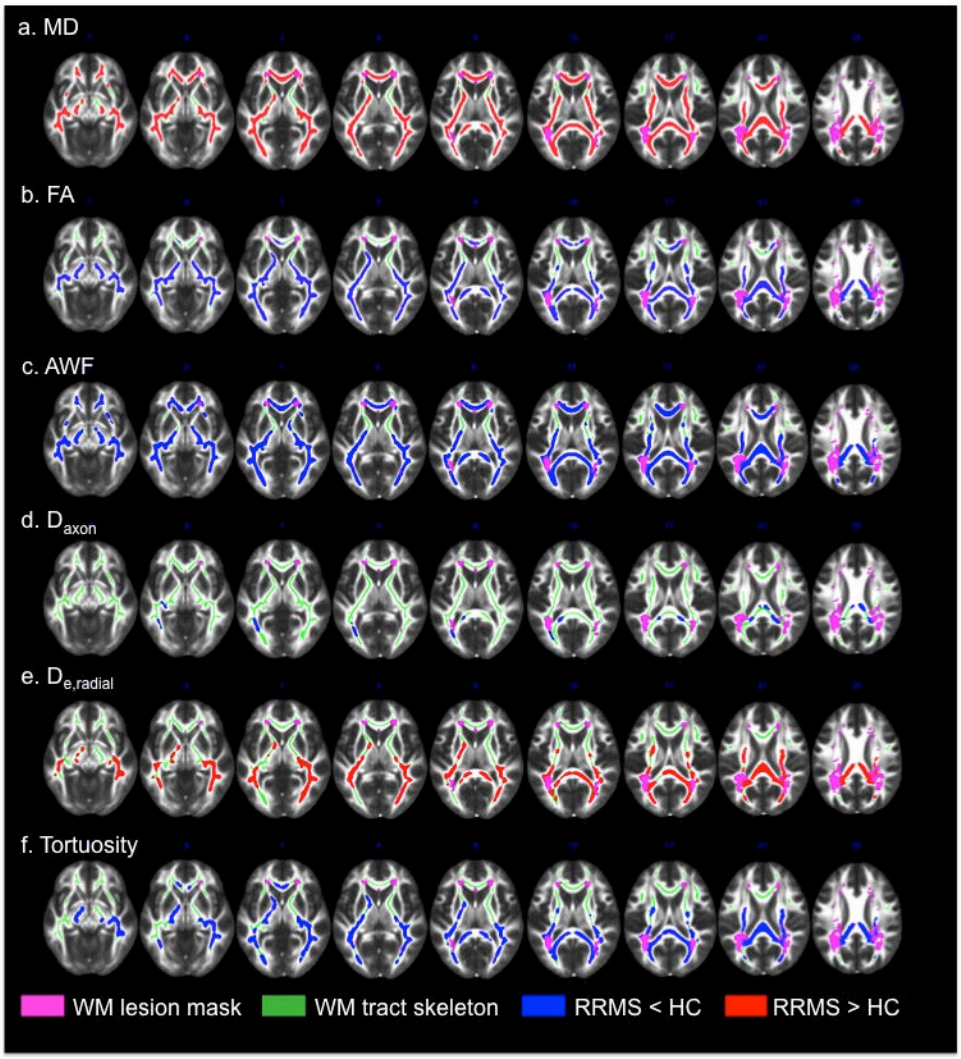

Fig. 2.

TBSS results showing statistically significant differences between RRMS and HC for the WMTI metrics of FA (a), MD (b), AWF (c), D_{axon} (d), $D_{e,radial}$ (e), and tortuosity (f). Clusters of voxels with significantly increased values (two-sided $P < .05$) in RRMS compared to HC (red), and significantly decreased values (blue) are overlaid on the FMRIB FA template together with the mean NAWM skeleton (green) and the lesion probability map (thresholded at > .1; pink)

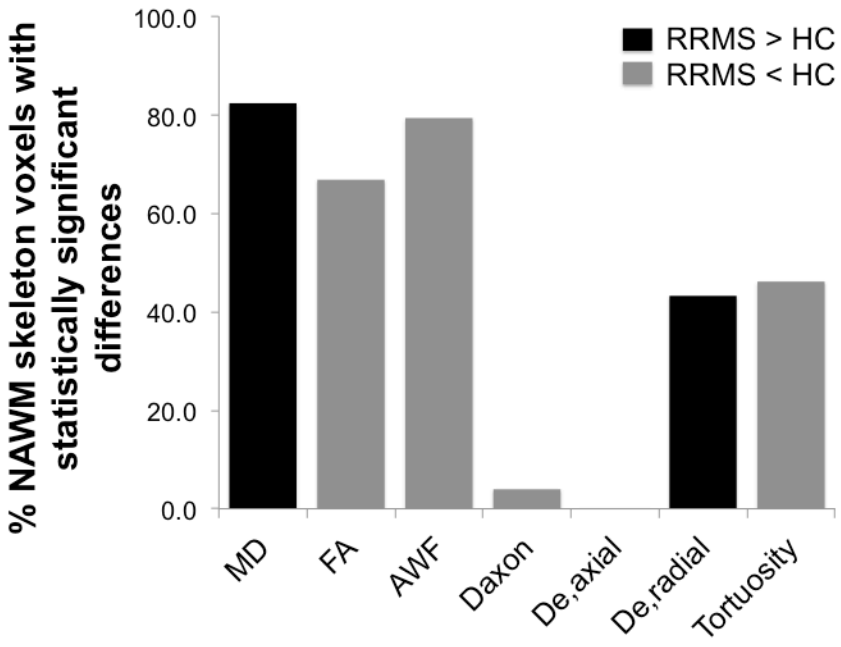

Fig. 3.

Bar graph representation of the percentage of NAWM skeleton voxels in RRMS patients with a statistically significant increase (black) or decrease (gray) in FA, MD, and WMTI metrics compared to HC

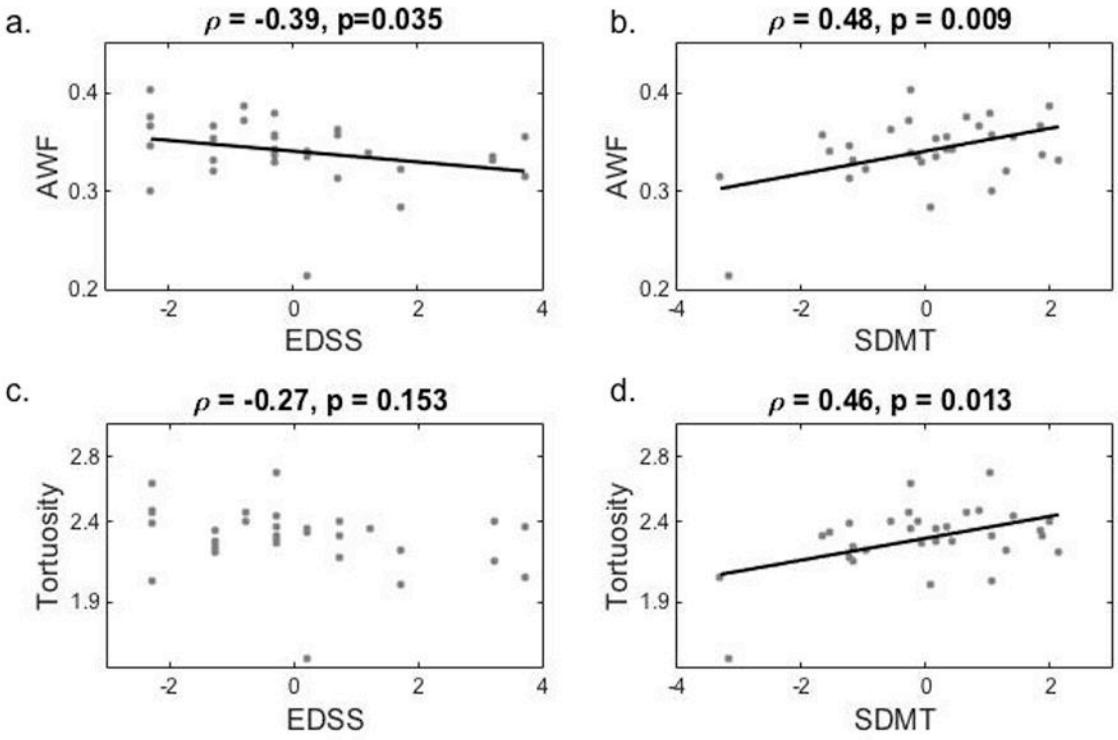

Fig. 4.

Mean axonal water fraction and tortuosity in the body of the corpus callosum as a function of EDSS (a and c, respectively) and SDMT (b and d, respectively) score, with best fit lines and corresponding Spearman rank (a and c) and Pearson (b and d) correlation coefficients

Table 1

Demographic, clinical and radiological characteristics of the study groups

	HC (n = 19)[a]	RRMS (n = 32)[a]
Females, n	13	24
Age, yrs	36.2 ±11.4	37.0 ±9.3
DD, yrs	-	3.6 ±3.9
EDSS, median score (range)	-	2 (0–6)
SDMT (Z score)		−0.73 ±1.36
T2LV, mL	-	3.10 ±7.93
T1LV, mL	-	0.90 ±2.27
CE, n	-	0.6 ±1.0

[a]All measures are reported as mean ± standard deviation (SD) unless otherwise specified.

Table 2

Group differences in the corpus callosum

		HC (n = 19)		RRMS (n = 32)			
Metric[a]	**ROI**	**Mean**	**STD**	**Mean**	**STD**	**P-value**[b]	**AUC**
MD	Genu	0.97	0.07	1.04	0.12	0.016	0.71
	Body	1.14	0.09	1.26	0.14	0.002	0.77
	Splenium	0.89	0.05	0.96	0.10	0.006	0.79
FA	Genu	0.57	0.03	0.54	0.05	0.014	0.72
	Body	0.55	0.06	0.52	0.05	0.048	0.74
	Splenium	0.61	0.03	0.58	0.06	0.027	0.75
AWF	Genu	0.41	0.03	0.38	0.04	0.004	0.77
	Body	0.38	0.03	0.34	0.03	<0.001	0.85
	Splenium	0.45	0.03	0.41	0.04	0.001	0.81
D_{axon}	Genu	1.01	0.06	0.99	0.08	0.414	0.60
	Body	1.10	0.06	1.07	0.08	0.163	0.67
	Splenium	1.09	0.07	1.05	0.10	0.173	0.64
$D_{e,axial}$	Genu	2.83	0.13	2.87	0.15	0.273	0.58
	Body	3.19	0.14	3.28	0.18	0.063	0.65
	Splenium	2.76	0.08	2.79	0.12	0.322	0.63
$D_{e,radial}$	Genu	1.16	0.11	1.26	0.18	0.030	0.66
	Body	1.40	0.13	1.55	0.21	0.008	0.72
	Splenium	1.03	0.09	1.13	0.17	0.025	0.71
Tortuosity	Genu	2.75	0.28	2.52	0.27	0.006	0.72
	Body	2.49	0.18	2.30	0.20	0.002	0.76
	Splenium	3.11	0.32	2.84	0.37	0.012	0.73

[a] MD, D_{axon}, $D_{e,axial}$ and $D_{e,radial}$ are reported in μm^2/ms. FA, AWF and Tortuosity are dimensionless.

[b] Obtained from analysis of covariance, correcting for age.